Materials Today Physics 38 (2023) 101267

Contents lists available at ScienceDirect

Materials Today Physics

journal homepage: www.journals.elsevier.com/materials-today-physics

Pressure-induced metallic state in a van der Waals cluster Mott insulator Nb_3Cl_8

P.F. Shan [a,b,1], X. Han [a,b,1], X. Li [d,**], Z.Y. Liu [a,b], P.T. Yang [a,b], B.S. Wang [a,b], J.F. Wang [c], H.Y. Liu [e], Y.G. Shi [a,b,f], J.P. Sun [a,b,*], J.-G. Cheng [a,b]

[a] Beijing National Laboratory for Condensed Matter Physics and Institute of Physics, Chinese Academy of Sciences, Beijing, 100190, China
[b] School of Physical Sciences, University of Chinese Academy of Sciences, Beijing, 100049, China
[c] Wuhan National High Magnetic Field Center, Huazhong University of Science and Technology, Wuhan, 430074, China
[d] Henan Institute of Advanced Technology, Zhengzhou University, Zhengzhou, 450001, China
[e] Key Laboratory of Material Simulation Methods and Software of Ministry of Education, College of Physics, Jilin University, Changchun, 130012, China
[f] Songshan Lake Materials Laboratory, Dongguan, Guangdong, 523808, China

ARTICLE INFO

Keywords:
Nb_3Cl_8
High pressure
Topological flat bands
Mott insulator

ABSTRACT

We report on the pressure-induced metallization of a van der Waals cluster Mott insulator Nb_3Cl_8 by employing the resistivity measurements under high pressure. Upon compression, its resistance and energy gap are suppressed gradually with exhibiting the fully metallic state at a critical pressure of $P_c \approx 70$ GPa. Hall resistance measurements revealed a significant band-structure reconstruction around P_c, where the dominant charge carriers are altered from hole-to electron-type and the carrier concentration experiences a sharp increase in the metallic state. In addition, high-pressure synchrotron XRD measurements uncover a possible structural phase transition around P_c. Our further first-principles calculations reproduced the pressure-driven structure transition and the corresponding metallic state above P_c. The present study demonstrates a feasible high-pressure route to realize the metallization of cluster Mott insulator Nb_3Cl_8.

1. Introduction

Mott insulators arise from strong on-site Coulomb interactions that split half-filled band into lower and upper Hubbard bands [1]. The unpaired localized electrons in Mott insulators also carry spin and/or orbital degrees of freedom and the strong interplay between them usually gives rise to complex ordered states at low temperatures [2]. On the other hand, metallization of Mott insulators, which delocalizes the charge carriers and strengthens the entanglement of these quantum degrees of freedom, can lead to more exotic emergent phenomena [3–5], such as the high-temperature superconductivity in cuprates [6] and the colossal magnetoresistance effect in the perovskite magnets [7]. Motivated by these celebrated discoveries, considerable effort has thus been devoted to exploring the metallization of Mott insulators during the last decades. In general, band-filling control and bandwidth control are two commonly used approaches to realize the transition from Mott insulator to metal. The former one introduces extra charge carriers and, in most cases, alters the magnetic and electronic ground states of the system via modifying band structure and the spin/orbital interactions; while the latter one utilizes a cleaner tuning knob, such as high pressure, to overcome the Coulomb interactions by broadening the Hubbard bandwidth. These approaches have been applied to metallize the cluster Mott insulators (CMIs) GaM_4Se_8 (M = Nb, Ta) with deficient spinel structures, leading to the discovery of superconductivity in the pressure-indued metallic state at low temperatures [8]. In the present work, here we report on the metallization of a newly discovered CMI Nb_3Cl_8 via applying the high-pressure approach.

As shown in the inset of Fig. 1(a), Nb_3Cl_8 adopts a layered structure with space group $P\bar{3}m1$ (No. 164) at ambient pressure (AP), consisting of Nb_3Cl_8 monolayers that are stacked along the c axis via the weak van der Waals force [9,10]. Within each monolayer, the Nb atoms form typical breathing Kagome lattice of Nb_3 trimers, with the intra-cluster Nb–Nb distances of d_1 = 2.834 Å and the inter-cluster Nb–Nb distances of d_2 = 3.998 Å, respectively. Upon cooling down at AP, the

* Corresponding author. Beijing National Laboratory for Condensed Matter Physics and Institute of Physics, Chinese Academy of Sciences, Beijing, 100190, China.
** Corresponding author.
E-mail addresses: lx2021@zzu.edu.cn (X. Li), jpsun@iphy.ac.cn (J.P. Sun).
[1] These authors contributed equally to this work.

https://doi.org/10.1016/j.mtphys.2023.101267
Received 30 August 2023; Received in revised form 18 October 2023; Accepted 20 October 2023
Available online 21 October 2023

magnetic susceptibility of Nb_3Cl_8 single crystals exhibit a magnetic-nonmagnetic phase transition at ~100 K, which can also be detected from the heat-capacity measurement [9,10]. According to the X-ray diffraction and nuclear magnetic resonance measurements, this phase transition is driven by a charge disproportionation that the uniform $[Nb_3]^{8+}$ trimers transform into $[Nb_3]^{7+}$ and $[Nb_3]^{9+}$ [9]. First-principles calculations show the existence of several topological flat bands below the Fermi level, which has been confirmed by the angle-resolved photoemission spectroscopy (ARPES) experiments [10]. Moreover, the electronic transport properties, spin configurations and band structures establish Nb_3Cl_8 as a candidate of Mott insulator [11–13]. The mechanism can be described that the Nb 4*d* orbitals first split into e_g and t_{2g} orbitals due to the octahedral crystal field and then the $[Nb_3]^{8+}$ trimers further form the molecular orbitals with six electrons filling the lowest $1a_1$ and $1e$ orbitals and unpaired seventh electron occupying the $2a_1$ orbital. Furthermore, the half-filled flat band of Nb_3Cl_8 splits to the upper and lower Hubbard bands with a significant gap opening and thus points that it should be a Mott insulator. Although much effort has been devoted to metallizing Nb_3Cl_8 by chemical doping [14,15], it remains unsuccessful so far. To this end, we resort to the high-pressure approach aiming at the metallization of this new CMI and further exploration of possible superconductivity.

Through detailed measurements of resistivity under high pressures up to 96 GPa, we find that the Mott insulating state of Nb_3Cl_8 can be suppressed gradually and a fully metallic state appears above a critical pressure of $P_c \approx 70$ GPa. The emergence of a metallic phase above P_c is accompanied with a significant band-structure reconstruction as well as crystal structure phase transition. All these results can be well reproduced by our DFT calculations. The present study thus demonstrates a feasible route to metallize the newly discovered cluster Mott insulator Nb_3Cl_8, which should be subjected to more experimental and theoretical investigations.

2. Experimental details

High quality single crystals of Nb_3Cl_8 were synthesized by using $PbCl_2$ as the flux. The Nb (Alfa Aesar, 99.99 %) and $NbCl_5$ (Alfa Aesar, 99.9 %) were mixed with a molar ratio of 7:8 in a glovebox as the starting materials. The alumina crucible was used to place the mixture and then was sealed in a quartz tube under vacuum. Then the single crystals were grown by heating the quartz tube to 750 °C for 150 h, and then cooled to room temperature slowly. Finally, the hot water was used to remove the excess $PbCl_2$ flux. High-pressure electrical transport measurements were performed in the BeCu-type diamond anvil cell (DAC) with 100 μm and 200 μm flat. KBr was used as the solid pressure transmitting medium (PTM). The size of single-crystal samples was about 40 × 40 × 5 μm^3. High-pressure synchrotron XRD measurements were performed in a symmetric DAC at the BL15U1 station of the Shanghai Synchrotron Radiation Facility (SSRF). Here, the 4:1 methanol/ethanol mixture was used as the PTM. The pressures in DAC were monitored at room temperature with the ruby fluorescence method and diamond Raman edge at higher pressure.

3. Results and discussion

Fig. 1 shows the in-plane resistance $R(T)$ data of CMI Nb_3Cl_8 (No. 1 and No. 2) measured under various high pressures up to 81 GPa and 96 GPa in the DAC apparatus. As can be seen in Fig. 1(a), the $R(T)$ of sample No. 1 exhibits an obvious insulating behavior from room temperature to 1.5 K at 36 GPa. When applying pressure to 54 GPa, the $R(T)$ in the whole temperature range decreases significantly in comparison to that at 36 GPa, and exhibits a weak temperature dependence with a metallic region in between 150 K and 70 K, followed by an upturn at lower temperatures. Upon increasing pressure to 81 GPa, the $R(T)$ is further reduced and changed to a typical metallic behavior. These results demonstrate that pressure can induce an insulator to metal transition in the CMI Nb_3Cl_8.

To track the detailed evolution of the pressure-induced insulator to metal transition in Nb_3Cl_8, we measured high-pressure resistance of another sample No. 2, which shows consistent results with the sample No. 1. As see in Fig. 1(b), the $R(T)$ at 28 GPa shows an obvious insulating behavior showing a quick rise of resistance by more than three orders of magnitude upon cooling down. The $R(T)$ decreases gradually with increasing pressure and the $R(T)$ at 60 GPa approaches the boundary to metallic state. It exhibits a weak insulating behavior at high temperatures and evolves to a metallic state followed by a weak upturn below ~80 K. At 68 GPa, the metallic region is enlarged, and the weak upturn is further suppressed to below ~20 K. When we further increase pressure to 79 GPa and above, the $R(T)$ curves exhibit typical metallic behavior, which can be seen more clearly in the inset of Fig. 1(b). Based on the above high-pressure transport results on the two samples, we confirm that the application of high pressure induces an insulator to metal transition in the CMI Nb_3Cl_8. However, no superconductivity was observed down to 1.5 K and up to ~100 GPa in the present study.

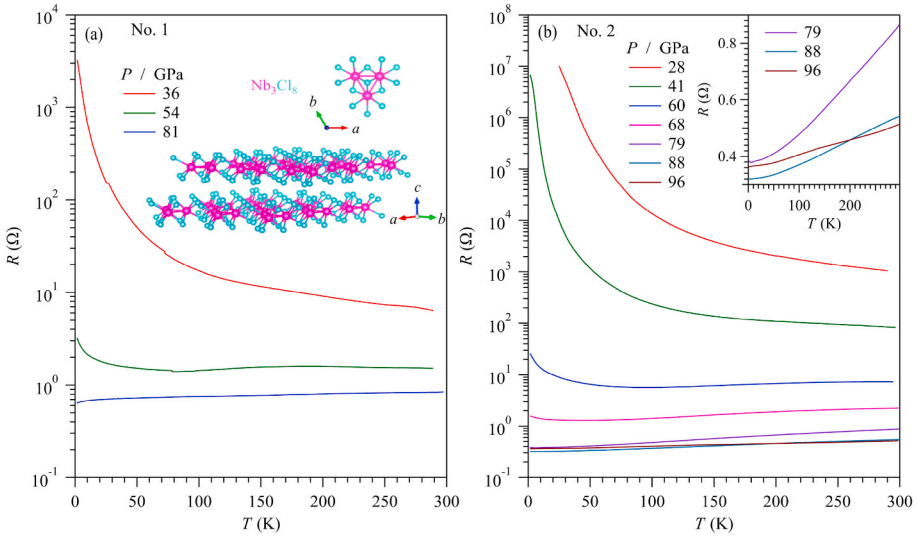

Fig. 1. Temperature dependences of resistance $R(T)$ for Nb_3Cl_8 single crystals (a) No. 1 with pressure between 36 GPa and 81 GPa and (b) No. 2 with pressure up to 96 GPa by using the DAC. The inset of Fig. 1(a) shows the crystal structure and top view of a Nb_3Cl_{13} cluster of Nb_3Cl_8, and the inset of Fig. 1(b) shows the temperature dependences of resistance $R(T)$ at 79 GPa, 88 GPa and 96 GPa.

As seen in Fig. 2(a), the resistance values at 290 K of sample No. 2 first decrease quickly by three orders of magnitude with increasing pressure from 28 to 79 GPa, and then levels off above 80 GPa in the metallic state. For the resistance $R(T)$ curves below 60 GPa, we employ the thermal activation model to extract the activation energy E_g, e.g., $R(T) = R_0\exp(E_g/k_BT)$, and the fitting results are shown in Fig. 2(b). The E_g decreases rapidly from ~1 eV estimated from ARPES data at ambient pressure to ~40 meV at 28 GPa, and then tends to be suppressed above 60 GPa. Accompanying with the sharp decrease of resistance $R(T)$ at room temperature, a sudden drop of energy gap was observed, signaling the occurrence of pressure-induced metallic state.

To further obtain the information of charge carriers, we perform the Hall resistance measurements from 60 GPa to 96 GPa at 100 K. The $R_{xy}(H)$ data were anti-symmetrized with respect to the magnetic field between +5 and −5 T. Fig. 2(c) and (d) show the Hall resistance $R_{xy}(H)$ at 100 K, and the normalized Hall coefficient and carrier density. As can be seen, the $R_{xy}(H)$ data show the linear dependence on magnetic field for all pressures. At 60 GPa and 68 GPa, the positive slope of $R_{xy}(H)$ indicates that the dominate carriers are hole-type. Above 70 GPa, the slope of $R_{xy}(H)$ changes to negative which implies that the electrons dominate the electrical transport behavior. Here, we employ the single band model to obtain the Hall coefficient by linear fitting to the $R_{xy}(H)$. Since the thickness of sample in DAC cannot be determined precisely, here we describe the relative changes of Hall coefficient $R_H(P)/R_H$(60 GPa) and carrier density $n(P)/n$(60 GPa). As displayed in Fig. 2(d), the Hall coefficient shows a sharp decrease with increasing pressure from 60 GPa to 79 GPa, which corresponds to the quick increase of the carrier density. Above 79 GPa, the carrier concentration decreases gradually in the metallic state. Thus, the analysis of Hall resistance further elaborated pressure-induced metallization of Nb_3Cl_8 accompanying with the dramatic increase of carrier densities around 80 GPa.

To probe the structural evolutions as a function of pressure, we measured the synchrotron XRD patterns of Nb_3Cl_8 at selected pressures up to 98 GPa, Fig. 3(a). Our results are consistent with previous reports which reported the merging of the (002) and (001) peaks below 6.5 GPa [16]. As is shown in the reports, the calculated bandgap experiences a sharp decrease at the structural transition from trigonal phase with three-fold rotational symmetry to the monoclinic phase with two-fold rotational symmetry near 7–8 GPa, but the resistance still exhibits strong insulating behavior up to ~20 GPa [16]. Here, we perform the XRD at higher pressures up to ~100 GPa to further construct the correlation between the pressure-induced metallic transport behaviors and the structure information. As can be seen, all the XRD peaks can be indexed by the space group $P\,\bar{3}\,m1$ (No. 164) at 0.7 GPa. When we increase the pressure gradually, all diffraction peaks shift to higher angles because of the lattice contraction. Here, we can see that no new Bragg peaks emerge up to 66 GPa (Fig. 3(a)). Due to the preferred orientation of the crystal grains and peak broadening under high pressure, some peaks are overlapped with adjacent peaks. Therefore, it's hard to deduce that whether there are structural phase transitions in this range. Upon further increasing pressure to 98 GPa, two new peaks located at a lower angle than the original two main peaks emerge above 73 GPa, as shown in Fig. 3(b), which indicates a pressure-induced structural phase transition. Considering the above resistance measurements, we speculate that the structure phase transition has an intimated correlation with pressure-induced insulator to metal transition. Unfortunately, the space group of the metallic phase cannot be accurately deduced from the high-pressure XRD measurements due to the peak broadening and the

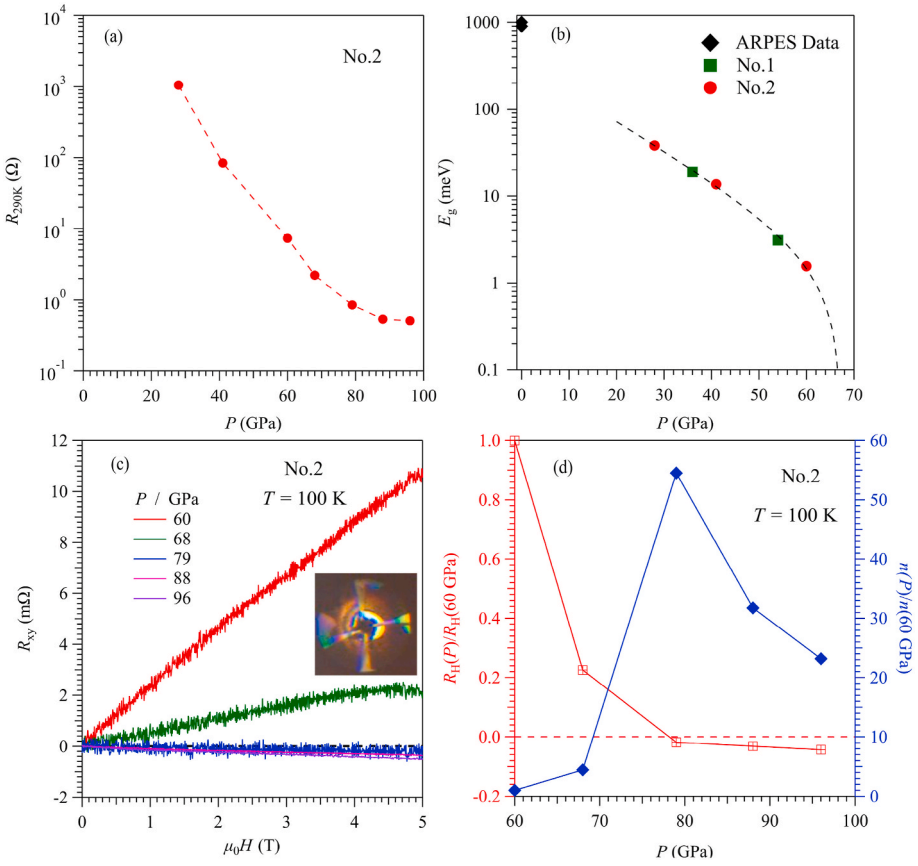

Fig. 2. (a) The resistance values R_{290K} at 290 K of Nb_3Cl_8 under various pressures up to 96 GPa for sample No. 2. (b) The pressure dependences of activation gap E_g for samples No. 1 and No. 2. The black diamond markers represent the E_g values extracted from the ARPES data, and the dash line is guided to eyes. (c) The Hall resistance R_{xy} of sample No. 2 at 100 K from 60 to 96 GPa. (d) The normalized Hall coefficient $R_H(P)/R_H$(60 GPa) and carrier density $n(P)/n$(60 GPa) for sample No. 2 as a function of pressure. The inset of (c) shows the arrangement of electrodes.

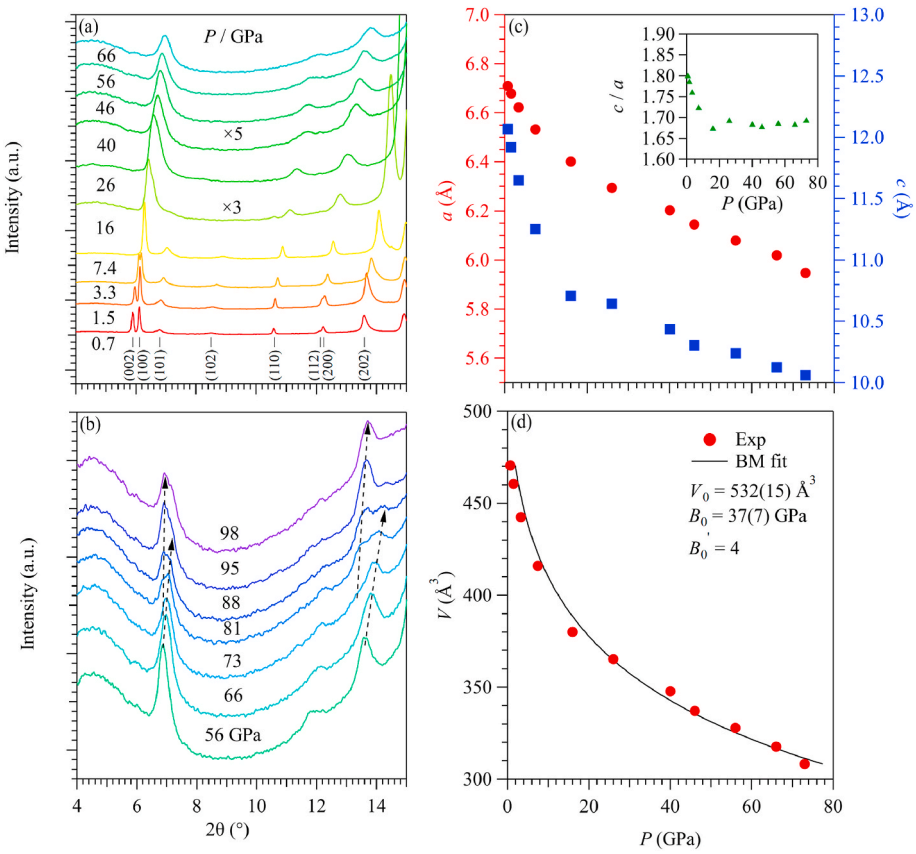

Fig. 3. (a) and (b) The synchrotron XRD patterns of Nb_3Cl_8 at selected pressures and room temperature. (c) Lattice parameters and (d) cell volume as a function of the pressure.

limited number of diffraction peaks above 70 GPa.

The XRD patterns were fitted with the LeBail method based on the ambient structure in the $P\,\bar{3}\,m1$ space group and the resulting lattice parameters and cell volume are displayed in Fig. 3(c) and (d). The lattice parameter a show a continuous decrease, while c exhibits a slope change at about ~16 GPa, leading to a strong reflection of c/a as seen in the inset of Fig. 3(c). The experimental $V(P)$ in Fig. 3(d) was fitted by employing the Birch-Murnaghan equation:

$$P(V)=\frac{3B_0}{2}\left[\left(\frac{V_0}{V}\right)^{7/3}-\left(\frac{V_0}{V}\right)^{5/3}\right]\left\{1+\frac{3}{4}\left(B_0^{'}-4\right)\left[\left(\frac{V_0}{V}\right)^{2/3}-1\right]\right\},$$

where V_0 is the unit cell volume at ambient pressure, V is the volume at pressure P, B_0 is the bulk modulus, and $B_0^{'}$ is a parameter for the pressure derivative. The calculated bulk modulus B_0 is about ~37(7) GPa with $B_0^{'}$ fixed at 4 and the ambient pressure unit cell volume V_0 is about ~532 (15) Å^3.

To resolve the crystal structure of Nb_3Cl_8 at higher pressures, we perform the structural searching for Nb_3Cl_8 at pressures of 80 GPa via swarm-intelligence-based CALYPSO structure prediction software [17–19]. The structural relaxation and properties evaluations were conducted with the framework of density functional theory (DFT) as implemented in the Vienna *ab initio* simulation Package (VASP) package within the Perdew-Burke-Ernzerhof (PBE) generalized gradient approximation as the exchange-correlation function [20–22]. The $4s^24p^64d^45s^1$ and $3s^23p^5$ configurations is chosen as valence electrons for Nb and Cl. The kinetic cutoff energy of 300 eV and dense k-point meshes with $2\pi \times 0.025$ Å^{-1} were chosen to ensure enthalpy better converged. The existing trigonal phase and newly predicted Monoclinic phase are shown in Fig. 4. Compared with the ambient structure of Nb_3Cl_8, the theoretical proposed $C2/m$-Nb_3Cl_8 phase holds denser atomic stacking and lowest enthalpy under high-pressure. For example, the central Nb atoms are surrounded by seven Cl atoms in $C2/m$-Nb_3Cl_8 (Fig. 4(b)), which is more than coordination numbers in P-3m1-Nb_3Cl_8 phase (Fig. 4(a)). At 80 GPa, the calculated lattice parameters are a = 13.66 Å, b = 2.79 Å and c = 7.06 Å, and the $\alpha = 90.00°$, $\beta = 86.97°$ and $\gamma = 90.00°$. With increasing pressure gradually, the average distance between Nb and Cl were decreased from 2.53 Å to 2.35 Å. Furthermore, we also calculated the density of states in the trigonal and monoclinic phases, and find that the newly proposed monoclinic phase exhibits intrinsic metallicity as displayed in Fig. 4(c and d), which is consistent with the high-pressure transport results.

The discovery of pressure-induced metallization in CMI Nb_3Cl_8 is quite encouraging and should stimulate more studies in this new two-dimensional van der Waals CMI family. Firstly, it represents a new class of CMI with unique two-dimensional crystal structure and in-plane breathing Kagome lattice. Unfortunately, the pressure-induced superconductivity was not observed in the pressure-induced metallic state of Nb_3Cl_8 up to ~100 GPa. Investigations at higher pressures should be performed to further explore whether the superconductivity can emerge. As mentioned above, the pressure-induced transition from Mott insulator to a superconductor is a rather rare phenomenon without a structural phase transition, and only be observed in the CMIs $GaNb_4Se_8$ and $GaTa_4Se_8$. More studies of chemical substitutions or carrier doping should be explored to further investigate the interplay between strong electron correlations and superconductivity in this CMI family. Secondly, it offers a new platform to study the insulator to metal transition and further understand the electronic behavior associated with the crossover from localized to itinerant electrons. As indicated by our study, the structural phase transition of Nb_3Cl_8 has not been determined experimentally above 70 GPa. In this regard, it is highly desirable to determine the crystal structure of Nb_3Cl_8 under high-pressure and then

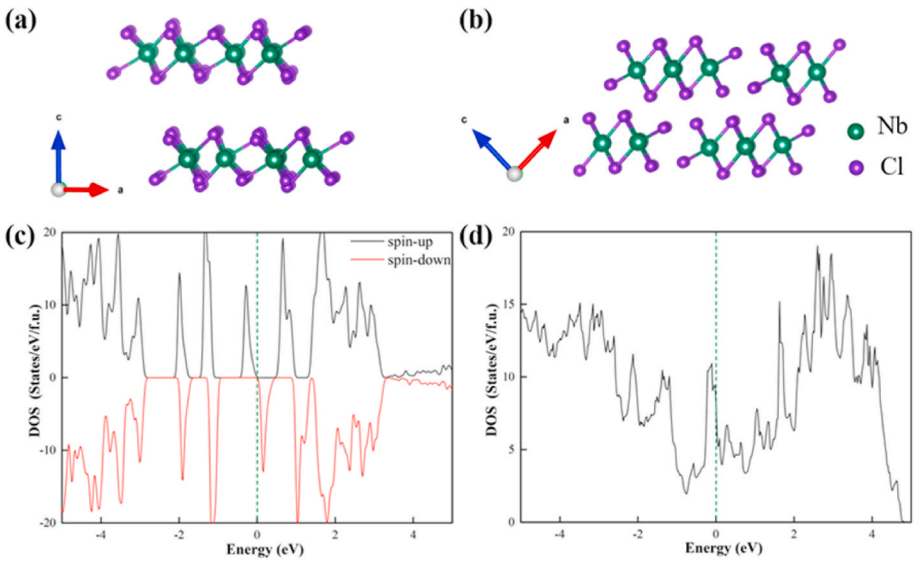

Fig. 4. Crystal structure of (a) *P*-3*m*1 -Nb_3Cl_8 and (b) *C*2/*m*-Nb_3Cl_8; Calculated electronic density of states for (c) *P*-3*m*1 -Nb_3Cl_8 and (d) *C*2/*m*-Nb_3Cl_8.

to reveal its evolution under high pressure.

4. Conclusion

In summary, we report on the pressure-induced metallization in the two-dimensional van der Waals CMI Nb_3Cl_8 above ~70–80 GPa by employing high-pressure transport measurements. Moreover, the metallic state is accompanied with the structural phase transition and the change of band structure, which is supported by the measurement of Hall resistance and XRD as well as DFT calculations. Our study demonstrates that the new family of CMI Nb_3Cl_8 can be metallized by compression and should be further explored via chemical substitutions and/or strain engineering.

Credit author statement

J. P. Sun and J. G. Cheng conceived this research and supervised the project. X. Han and Y. G. Shi synthesized the Nb3Cl8 single crystals. P. F. Shan, Z. Y. Liu, P. T. Yang, B. S. Wang and J. P. Sun did the high-pressure transport measurement. P. F. Shan did the synchrotron x-ray diffraction. X. Li and H. Y. Liu did the structural searching and the theoretical calculations. P. F. Shan and J. P. Sun prepared the original manuscript draft. Then J. P. Sun and J. G. Cheng made further revision. All authors discussed the results and made comments.

Declaration of competing interest

The authors declare that they have no known competing financial interests or personal relationships that could have appeared to influence the work reported in this paper.

Data availability

Data will be made available on request.

Acknowledgements

This work is supported by the National Key R&D Program of China (2021YFA1400200 and 2022YFA1403900), the National Natural Science Foundation of China (Grant Nos. 12025408, 12174424 and 11921004), the Strategic Priority Research Program and Key Research Program of Frontier Sciences of CAS (XDB33000000), the Youth Innovation Promotion Association (No. 2023007), the K. C. Wong Education Foundation (GJTD-2020-01), the Interdisciplinary program of Wuhan National High Magnetic Field Center (Grant No. WHMFC202204), and Users with Excellence Program of Hefei Science Center CAS (Grant No. 2021HSC-UE008). High-pressure XRD measurements were performed at the BL15U1 station of the Shanghai Synchrotron Radiation Facility (SSRF).

References

[1] N.F. Mott, Metal-insulator transitions, Pure Appl. Chem. 52 (1979) 65.
[2] M. Imada, A. Fujimori, Y. Tokura, Metal-insulator transitions, Rev. Mod. Phys. 70 (1998) 1039.
[3] E. Dagotto, Complexity in strongly correlated electronic systems, Science 309 (2005) 257.
[4] P.A. Lee, N. Nagaosa, X.-G. Wen, Doping a Mott insulator: physics of high-temperature superconductivity, Rev. Mod. Phys. 78 (2006) 17.
[5] J.B. Goodenough, Electronic and ionic transport properties and other physical aspects of perovskites, Rep. Prog. Phys. 67 (2004) 1915.
[6] J.G. Bednorz, K.A. Müller, Possible high T_c superconductivity in the BaLaCuO system, Z. Phys. B 64 (1986) 189.
[7] R. von Helmolt, J. Wecker, B. Holzapfel, L. Schultz, K. Samwer, Giant negative magnetoresistance in perovskitelike $La_{2/3}Ba_{1/3}MnO_x$ ferromagnetic films, Phys. Rev. Lett. 71 (1993) 2331.
[8] M.M. Abd-Elmeguid, B. Ni, D.I. Khomskii, R. Pocha, D. Johrendt, X. Wang, K. Syassen, Transition from Mott insulator to superconductor in $GaNb_4Se_8$ and $GaTa_4Se_8$ under high pressure, Phys. Rev. Lett. 93 (2004): 126403.
[9] Y. Haraguchi, C. Michioka, M. Ishikawa, Y. Nakano, H. Yamochi, H. Ueda, K. Yoshimura, Magnetic–Nonmagnetic phase transition with interlayer charge disproportionation of Nb_3 trimers in the cluster compound Nb_3Cl_8, Inorg. Chem. 56 (2017) 3483.
[10] Z.Y. Sun, H. Zhou, C.X. Wang, S. Kumar, D.Y. Geng, S.S. Yue, X. Han, Y. Haraguchi, K. Shimada, P. Cheng, L. Chen, Y.G. Shi, K.H. Wu, S. Meng, B.J. Feng, Observation of topological flat bands in the kagome semiconductor Nb_3Cl_8, Nano Lett. 22 (2022) 4596.
[11] S.Y. Gao, S. Zhang, C.X. Wang, W. Tao, J.T. Liu, T.T. Wang, S.K. Yuan, G.X. Qu, M. J. Pan, S.Y. Peng, Y. Hu, H. Li, Y.B. Huang, H. Zhou, S. Meng, L. Yang, Z.W. Wang, Y.Y. G, Z.G. Chen, M. Shi, H. Ding, K. Jiang, Y.L. Li, Y.G. Shi, H.M. Weng, T. Qian, Mott insulator state in a van der Waals flat-band compound, arXiv: 2205 (2022): 11462.
[12] S. Regmi, T. Fernando, Y.Z. Zhao, A.P. Sakhya, G. Dhakal, I.B. Elius, H. Vazquez, J. D. Denlinger, J.H. Yang, J.H. Chu, X.D. Xu, T. Cao, M. Neupane, Spectroscopic evidence of flat bands in breathing kagome semiconductor Nb_3I_8, Commun. Mater. 3 (2022) 100.
[13] Y. Zhang, Y.H. Gu, H.M. Weng, K. Jiang, J.P. Hu, Mottness in two-dimensional van der Waals Nb_3X_8 monolayers (X = Cl, Br, and I), Phys. Rev. B 107 (2022): 035126.
[14] C.M. Pasco, I.E. Baggari, E. Bianco, L.F. Kourkoutis, T.M. McQueen, Tunable magnetic transition to a singlet ground state in a 2D van der Waals layered Trimerized Kagomé magnet, ACS Nano 13 (2019) 9457.
[15] J. Yoon, E. Lesne, K. Sklarek, J. Sheckelton, C. Pasco, S.S.P. Parkin, T.M. McQueen, M.N. Ali, Anomalous thickness-dependent electrical conductivity in van der Waals layered transition metal halide, Nb_3Cl_8, J. Phys. Condens. Matter 32 (2020): 304004.

[16] Z.M. Jiang, D.Q. Jiang, Y.M. Wang, C. Li, K. Liu, T. Wen, F.Y. Liu, Z.Y. Zhou, Y. G. Wang, Pressure-driven symmetry breaking and electron disproportionation of the trigonal Nb_3 cluster in Nb_3Cl_8, Sci. China Phys. Mech. Astron. 65 (2022): 278211.
[17] Y.C. Wang, J. Lv, L. Zhu, Y.M. Ma, Crystal structure prediction via particle-swarm optimization, Phys. Rev. B 82 (2010): 094116.
[18] Y.C. Wang, J. Lv, L. Zhu, Y.M. Ma, CALYPSO: a method for crystal structure prediction, Comput. Phys. Commun. 183 (2012) 2063.
[19] X.C. Shao, J. Lv, P. Liu, S. Shao, P.Y. Gao, H.Y. Liu, Y.C. Wang, Y.M. Ma, A symmetry-orientated divide-and-conquer method for crystal structure prediction, J. Chem. Phys. 156 (2022): 014105.
[20] J.P. Perdew, Y. Wang, Accurate and simple analytic representation of the electron-gas correlation energy, Phys. Rev. B 45 (1992): 13244.
[21] G. Kresse, J. Furthmüller, Efficient iterative schemes for ab initio total-energy calculations using a plane-wave basis set, Phys. Rev. B 54 (1996): 11169.
[22] J.P. Perdew, K. Burke, M. Ernzerhof, Generalized gradient approximation made simple, Phys. Rev. Lett. 77 (1996) 3865.